Published in final edited form as:
Radiology. 2008 February ; 246(2): 434–443.

Radiation Dose to Organs and Tissues from Mammography: Monte Carlo and Phantom Study

Ioannis Sechopoulos, Ph.D.[1,2], **Sankararaman Suryanarayanan, M.B.A., Ph.D.**[1], **Srinivasan Vedantham, Ph.D.**[1], **Carl J. D'Orsi, M.D.**[1], and **Andrew Karellas, Ph.D.**[1,2]

1 *Emory University School of Medicine, Department of Radiology and Winship Cancer Institute, 1701 Uppergate Drive, Suite 5018, Atlanta, GA 30322*

2 *Georgia Institute of Technology, Wallace H. Coulter Department of Biomedical Engineering, 313 Ferst Drive, Atlanta, GA 30332*

Abstract

Purpose—To prospectively determine the radiation dose to the organs of the body during a standard bilateral two-view mammogram using Monte Carlo simulations and a phantom.

Materials and Methods—A modified version of the Cristy mathematical anthropomorphic phantom was implemented in the Geant4 Monte Carlo toolkit to simulate the conditions present in screen-film and digital mammography. The breast was simulated under compression in both the cranio-caudal and the medio-lateral oblique views. X-rays were tracked from the source until their absorption in the body, in the detector or their exit from the simulation limits, recording all the intermediate interactions in the body. The simulation was performed with x-rays of energy ranging from 6 to 35 keV to obtain results for clinically relevant spectra. The ratio of dose to each organ per unit dose to the breast, denoted the relative organ dose (ROD) was computed. The effect of using a body protective shield was also investigated.

Results—The organs that received a ROD higher than 0.10% in at least one view and one spectrum were the contralateral breast, ipsilateral eye and eye lens, heart, ipsilateral lung, and thymus. Among the organs, the maximum ROD found was 0.62%. The maximum ROD for the bone surfaces was 2.36% and for the red bone marrow was 0.56%. The highest ROD measured for the uterus and fetus at the first trimester was $<10^{-5}$.

Discussion—The radiation dose to all tissues other than the breast is extremely low. The dose to the first-trimester fetus is minimal.

INTRODUCTION

Although the radiation dose to the imaged breast during a standard mammographic acquisition is well known (1–8), the dose received by the other organs and tissues of the body from a mammographic procedure are not as well known. Data about organ dose during mammographic acquisition will help the study of issues relating to the safety of mammograms during pregnancy (9), and the epidemiological study of radiation related onset of specific diseases (10). In more practical terms, radiologists have adequate data to communicate the radiation dose delivered to the breast in mammography but no detailed data are available on

Corresponding Author: Andrew Karellas, Ph.D., Tel: (404)712-2411, Fax: (404)712-5813, E-mail: Andrew.Karellas@umassmed.edu.

radiation dose to other tissues as a result of this procedure. This information is important for patients who were not aware they were pregnant at the time of the procedure and for pregnant women with suspected breast abnormalities that may warrant mammography. To our knowledge, only one study (11) has been published on the radiation dose to the other organs of the human body from a mammographic procedure. That study, using a phantom and thermoluminescence dosimetry, reported the measured dose in a limited number of organs and tissues. Thus, the purpose of our study was to prospectively determine the radiation dose to the organs of the body during a standard bilateral two-view mammogram using Monte Carlo simulations and a phantom.

MATERIALS AND METHODS

With the use of the Geant4 toolkit (12,13) for Monte Carlo simulations, a C++ computer program was implemented by one of the authors (I.S.) to simulate the acquisition of a standard two view bilateral mammogram. The simulation included a representation of the human body based on the current version of the Cristy phantom (14), developed by Cristy and Eckerman (15) at the Oak Ridge National Laboratory (ORNL). In addition to the anthropomorphic phantom, the simulation included an x-ray point source as an approximation of the focal spot of the mammographic x-ray tube, the breast compression plate, the breast support plate, and the x-ray detector with cover plate.

Anthropomorphic phantom

The Cristy phantom consists of a representation of the human body and its organs with the use of geometrical shapes based on mathematical formulas. With the use of different parameters for the formulas the phantom is adjusted to represent a human body of six different ages. The phantom used in this study is that which represents an adult female (denoted in the ORNL report as “15-AF”).

In our implementation of the Cristy phantom (Figure 1), some modifications were made to enhance the simulation, adapt the geometrical shapes to Geant4’s capabilities, and to recreate the conditions during a mammogram. The major modifications, based on data from the International Commission on Radiological Protection (ICRP) Publication 89 (16) and the International Commission on Radiation Units and Measurements (ICRU) Report 46 (17) and anatomy literature (18), were the use of different elemental compositions and densities for each tissue, and the addition of the eyes, eye lenses and sternum to the phantom. Two geometrical adaptations were introduced in the phantom to allow for a simpler implementation in Geant4. These were the re-orientation of the legs so that their long axis was vertical as opposed to at an angle as in the original description, and the cross-section of the tori representing the sigmoid colon were circular, as opposed to elliptical. These two geometrical modifications were estimated to have a negligible impact on the results, given the expected low radiation levels reaching the lower portion of the phantom. The adaptations necessary to recreate the conditions during a mammographic study were simulating the imaged breast as compressed either horizontally for the cranio-caudal (CC) view or at an angle for the medio-lateral oblique (MLO) view, and rotating the head of the phantom towards the opposite side of the imaged breast in the CC view. The anthropomorphic phantom in this simulation had a total of 66 organs, bones, skin sections and other soft tissues (Table 1).

The compressed breast in the CC view was modeled as a semicircular cylinder with rounded edges with a radius (chest-wall to nipple distance) of 10 cm and a thickness of 5.2 cm. This size represents a mean breast in the CC view (19). The compressed breast in the MLO view was similar to that reported by Sechopoulos et al (20,21), with a compressed thickness of 5.7 cm, and a chest-wall to nipple distance (CND) of 10.2 cm. The thickness of the MLO view breast was chosen to be approximately 10% thicker than that of the CC view (22,23), while

the CND was chosen so that the mass of the breast tissue was equal to that in the CC view. The breast in both views was implemented as a homogeneous mixture of 50% glandular and 50% adipose tissue, as described by Hammerstein et al (1). The elemental composition of the pectoralis muscle used in the MLO view breast was specified as that of skeletal muscle (24). The contents of the organs of the digestive system were specified as water, while the content of the heart was specified as blood.

To characterize the variation in organ dose with compressed breast thickness, the Monte Carlo simulations were repeated for thin (2 cm thick in the CC view and 2.2 cm in the MLO view) and thick (8 cm CC view and 8.5 cm MLO view) breasts.

Monte Carlo simulation

To simulate the acquisition of a standard mammogram, the x-ray source, compression and support plates, and detector were placed in the appropriate location according to the simulated mammographic view and the imaged breast. For both views, the source-to-imager distance (SID) was set at 66 cm, and the air gap at 1.5 cm. At each energy level sixty million monochromatic x-rays were emitted from the point source towards a random location on the detector surface so that the x-ray field at the detector surface was uniform and congruent with the detector edges. The path traveled by the x-rays was followed until the x-ray either exited the simulation limits or was completely absorbed. The energy lost by the x-ray at each interaction, along with the organ in which the deposition took place, was recorded. The total energy deposited in the imaged breast was used to compute the glandular dose (D_g (E)) as described by Boone (7) with the suggestion of Wilkinson and Heggie (25), while the total energy deposited in the other organs was divided by each organ's mass to obtain the dose to each organ. The simulation was repeated with monochromatic x-rays of energies ranging from 6 to 35 keV in 1 keV steps. Due to the asymmetry of the distribution of the organs, the simulations were repeated for both breasts. The monochromatic results were interpolated to 0.5 keV resolution and combined by weighing them with the relative number of photons in each spectrum studied. The dose to each organ was normalized to that of the glandular dose to the breast, resulting in the relative organ dose (ROD), representing the dose to an organ in the body per unit glandular dose to the breast. The simulations were performed on a computer cluster consisting of 128 AMD Opteron 2.2 GHz processors (Advanced Micro Devices, Inc., Sunnyvale, CA).

To measure the resulting uncertainty in the results due to the random nature of Monte Carlo simulations, the simulations of the two views of the left breast were repeated five times, and the coefficient of variation (COV = $100\sigma/\mu$) of the ROD for all the organs was computed for the x-ray spectra with the least total number of x-rays (Mo/Mo 25 kVp) and with the highest total number of x-rays (Rh/Rh 35 kVp).

Computation of dose to the red bone marrow and the bone surfaces

Bone dosimetry is affected by the complex microscopic histological features of the bones which are impossible to account for in macroscopic Monte Carlo simulations. Therefore, the development of methodologies to compute dose to the bone surfaces (BS) and to the red bone marrow (RBM) from macroscopic data has been an issue of intense research (26–33). In our study, the dose to the RBM was estimated by one of the authors (I.S.) using the three-parameter mass-energy absorption coefficient ratio method (MEAC) (26–28,33). This method has been shown to obtain results comparable to all other methods applicable to a macroscopic Monte Carlo simulation (33). To compute the dose to the BS, the homogeneous bone approximation (HBA) (33) was used, which assigns the dose to the BS as the dose to the whole homogeneous bone volume. These two methods have been shown to overestimate the dose to the RBM and

BS at the low energy range, so the results in this study represent a conservative upper limit (33).

Computation of tissue dose and effective dose

Using the computed ROD, an example calculation of the total dose to the organs, bones and skin sections resulting from a standard one breast two-view mammogram was computed. To perform this calculation, it was assumed that the CC view acquisition results in a glandular dose to the breast of 2 mGy, while the MLO view results in a glandular dose of 2.5 mGy.

Using the dose to each organ found from the Monte Carlo simulations, the effective dose was calculated by one of the authors (I.S.) using both the current recommended tissue weighting factors based on ICRP Publication 60 (34) and the new proposed ICRP recommendations posted on the ICRP website on January 12, 2007 (35). The effective dose was computed in both cases for a complete mammographic examination (two views, both breasts) per unit glandular dose to both breasts.

Study of possible dose reduction with a lead shield

To study the possibility of reducing the radiation dose to the organs of the body, a virtual 0.25 mm thick lead shield between the simulated patient and the x-ray field was included in the simulations. In the simulation the shield was implemented as transparent to the x-rays, but the fact that the x-ray had entered the shield was recorded. With this record, a second computation of the dose to the organs was performed automatically by the Monte Carlo program, in which the dose deposited in the organs by x-rays that were flagged as having entered the shield was ignored. This allowed for the simultaneous computation of the dose to the organs with and without shield. The only assumption necessary for this algorithm to work was that the lead shield was thick enough to absorb all x-rays that entered it. This was accomplished by simulating the shield as having a thickness of 0.25 mm, which results in an absorption of 99.7% of x-rays of 35 keV.

The shield was simulated as large enough to cover the whole body, with an opening for the imaged breast with length along the chest-wall of 20 cm and a variable height of 6 cm larger than the breast thickness.

Validation

The breast in the CC view was modified to match the geometry reported by Boone (8), and the simulations were repeated with one million monochromatic x-rays from 6 to 35 keV, in 1 keV steps. The resulting glandular dose to the breast was compared to the results reported in that study. The mean deviation between our data and the fit equation reported by Boone was 7.2%.

The ability of the Monte Carlo simulation in predicting the dose levels to the organs and tissues outside the primary x-ray field is pointed to by previous validations of the Geant4 toolkit's simulations of the conditions present in mammography. The total linear attenuation coefficients, as well as the individual linear attenuation coefficients of the three relevant physical interactions between x-rays and soft tissue, used by Geant4 were reported to be previously validated against data from the National Institute of Standards and Technology (NIST) (20). In addition, the x-ray scatter functions in mammography used by Geant4 have also been previously validated (21,36,37), pointing to the applicability of this package in the study of dosimetry related to x-rays scattered in the breast.

RESULTS

Tables 2 (CC view) and 3 (MLO view) show the ROD value for the organs, bones (discriminated into bone surfaces and red bone marrow), and skin sections that received a ROD of 0.10% or higher in at least one view and one spectrum and for the uterus. Dose values that resulted in a ROD lower than this level were deemed negligible and are not shown for space considerations. For most volumes the ROD was found to remain constant after varying which breast was imaged. For these volumes the mean ROD is reported. For the volumes for which a different ROD was found depending on which breast was imaged, both values are shown. The simulated spectra (38) used and their first half value layers are also listed in Table 2 and 3. The negligible dose levels received by the phantom's legs and sigmoid colon confirm the minimal impact of the two geometrical modifications introduced in the design of the anthropomorphic phantom. Table 4 shows the results of the example calculation of total dose to the organs from a standard one breast two-view mammogram.

The variations in ROD values for the thinner and thicker breasts compared to the mean breast were found to be mainly due to the variations in the glandular dose to the imaged breasts (the normalizing value), not due to variations in the magnitude of the dose deposited in the different organs and tissues. Only the dose to the sternum in the MLO view was found to vary substantially with thickness, decreasing to 0.75 of the original magnitude for the simulation with the thin breast, while increasing to 1.28 of the original magnitude for the simulation with the thick breast. The magnitude of the dose deposited on all other organs and tissues listed in Tables 2 and 3 were found to remain approximately constant. Therefore, the ROD for these organs and tissues vary inversely with the variation of glandular dose to the imaged breast, for which previously reported values may be used (2–8,20).

The coefficients of variation of the ROD of the organs listed in Table 2 and 3, found by repeating the Monte Carlo simulations of the mammograms of the left breast, are listed in Table 5. From these values it can be seen that the uncertainties of the ROD for most organs is less than 5%. Although the number of x-rays that deposit energy in the eye lens is very low, resulting in a high COV, the lens' small mass results in a ROD high enough to include this volume in Tables 2 and 3. Due to the high COV found for the uterus volume, the ROD reported in Tables 2 and 3 specify only the order of magnitude of the ROD computed, not specific values, since the uncertainty is relatively high.

The effective dose computations yielded values of 0.0517 mSv/mGy (or mrem/mrad), using the current recommended tissue weighting factors, while with the new draft weighting factors the value found was 0.123 mSv/mGy (or mrem/mrad). These values varied by a maximum of 0.26% for the nine spectra used in our study. The value for the effective dose in mammography using the ICRP Publication 60 recommendations was found to be approximately within 2.3% of that reported by Hatziioannou et al (11).

With the lead shield present, the ROD of the organs that received the highest dose was not lowered substantially (Table 6). The impact on ROD by the presence of the lead shield was found to be approximately independent of the x-ray spectrum used and the breast imaged, so Table 6 shows the mean of the ratio of ROD with the lead shield over ROD without the lead shield. The contralateral breast in the CC view, and the heart, the ipsilateral lung and the thymus in both views were minimally protected by the shield. The dose to the contralateral breast in the MLO view was reduced to a third of the dose without the shield, while the dose to the ipsilateral eye and eye lens in both views were almost completely eliminated. The dose to the uterus was reduced by approximately a factor of seven in the CC view and a factor of two in the MLO view by the presence of the shield. Of the bones, only the ipsilateral clavicle in the CC view was well protected.

DISCUSSION

As can be seen from the results, all organs outside the primary x-ray field receive less than 0.7% of the glandular dose received by the imaged breast. Except for the contralateral breast, the organs that absorb the most dose from a mammogram are the eye lens and the lung, with maximum ROD of 0.16% and 0.12%. Considering the x-ray spectrum that results in the maximum dose deposition to the lungs (Rh/Rh 35 kVp), the dose deposited in the lungs during a complete two-view bilateral mammographic study is approximately 4.8 μGy. This is equivalent to approximately one fortieth of the dose to the lungs from a chest radiograph (39), and one five hundredth to one three thousandth of the dose to the lungs from a single chest CT scan (40,41). For the red bone marrow, the maximum ROD found was 0.56%, while the maximum ROD for the bone surfaces was 2.36%. The results for both the bone marrow and the bone surfaces can be taken as a conservative upper limit, since at these energy levels it has been found that the methods used in our study tend to overestimate the dose (33). Therefore, in standard mammography, the dose to the organs and skeleton outside the primary x-ray field, including the fetus and ovaries, is minimal, if not negligible.

As expected, compared to the glandular dose, the skin of the imaged breast receives a much higher dose, which becomes lower with increasing x-ray spectrum energy. If only the portion of the breast skin facing the x-ray tube is considered, its local dose can be approximated to be double that specified for the whole breast skin. The dose to the skin of the contralateral breast (1.5%–2.2%) can normally be ignored since that same skin will receive the full dose when the contralateral breast is being imaged.

In our study, it was found that the dose to the uterus due to an average two-view bilateral mammogram is less than 0.03 μGy (0.003 mrad) per imaged breast. This result can be representative of the dose to the fetus during the first trimester, when the volume of the uterus as simulated in our study is still representative of that of a pregnant woman and the conceptus is very small. This amount of dose to the fetus is approximately 100 to 700 times lower than that received by the fetus from a helical chest CT scan of a pregnant patient (42). Even though the dose to the fetus from a mammogram can be considered to be minimal, the use of a lead shield reduces this dose further by about a factor of between two and seven. Therefore, if a patient underwent a standard mammogram not knowing that she was in the early stages of pregnancy, our findings suggest that the dose to the fetus is minimal. If, however, a patient is known to be pregnant and a mammogram is deemed necessary, a lead apron can lower this low amount of dose to the fetus by at least one half.

The shield results show that most of the dose to the organs is a consequence of x-rays that scatter in the breast tissue and enter the trunk through the breast, minimizing the benefit of using a lead shield or apron under normal circumstances.

The results from the simulations performed with breasts of different thicknesses show no substantial variation in the dose to the organs with varying breast thickness, except for the dose to the sternum in the MLO view. This can be explained by the fact that most of the x-rays entering the imaged breast are absorbed or scattered in the first layers of breast tissue, therefore, the introduction or removal of breast tissue does not contribute substantially to the number of x-rays scattering out of the breast towards the rest of the body. With varying compressed breast thickness in the MLO view, the proximity of the top layer of the breast to the sternum varies, resulting in the substantial variation found in the dose to the sternum in this view.

A limitation of our study is that the results depend on the applicability of the mathematical phantom as representative of the human body. Although this phantom is used extensively for dosimetry in radiology, its simplification of the shapes of the organs of the human body has the potential of introducing severe errors in the results, particularly with patients with body

habitus that greatly deviates from the assumed shape of the phantom. However, a recent study by Castellano et al (43), comparing the dose estimations of the Cristy phantom to a voxel based phantom from CT acquisitions has found the disagreements between the two phantoms to be less than 38%, and within 15% if the imaged sections of the phantoms are matched appropriately. Although these deviations are considerable, the importance or lack thereof of the dose to the different organs from mammography found in our study is still applicable since an increase in ROD by 40% would still result in maxima of 0.17% (ipsilateral lung), 0.78% (sternum bone marrow) and 3.30% (sternum bone surface). The effective dose computations, even with the additional 40% in the dose to all the organs except the imaged breast, is still valid, since the breast accounts for over 96% of the effective dose.

Another limitation is that two sources of radiation were not taken into account in our study: x-ray leakage from the shielded portions of the x-ray tube, and the fraction of x-rays from the primary field that are transmitted through the imager support arm. According to the U.S. Code of Federal Regulations (21CFR1020.31), the x-ray leakage in a mammography system must be limited to a maximum air kerma of 0.88 mGy (100 mR exposure) per hour at 1.0 meter from the source. Approximating a bilateral two-view mammogram to entail six seconds of x-ray exposure, the air kerma at 1 m from the focal spot from leakage radiation must be less than 1.5 μGy (0.167 mR exposure). The same chapter of the U.S. Code of Federal Regulations limits the radiation transmitted through the imager support arm to 0.88 μGy air kerma (0.1 mR exposure) 5 cm under the support arm per acquisition. Therefore, the radiation from tube leakage and primary barrier transmission is well within the uncertainty level of our study.

In summary, using Monte Carlo methods and a modified anthropomorphic geometrical phantom, a simulation of the conditions present during a standard mammographic acquisition was implemented and used to compute the radiation dose levels received by 66 different volumes representing the organs of the body during both CC and MLO view acquisitions. The dose to the organs and tissues located outside the primary x-ray field was found to be very low.

Practical Application

The results of our study indicate the radiation dose levels received by the organs and tissues of the body from standard mammography. This information may be used by epidemiologists studying the risks involved in screening and diagnostic mammography and by radiologists to assuage patients' concerns about the amount of radiation exposure during mammography. Furthermore, since the dose to the uterus was found to be extremely low, a mammographic procedure, especially with the use of a lead apron, may be considered by the radiologist faced with a pregnant patient with a possible breast cancer diagnosis.

Advances in Knowledge

1. Based on our Monte Carlo and phantom study, the radiation dose to the organs and tissues of the body outside the primary x-ray field from standard mammography was found to be very low (less than 2.5% of the average glandular dose to the imaged breast).
2. The uterus is exposed to extremely low dose levels (less than 10^{-5} of the average glandular dose to the imaged breast) during standard mammography, resulting in equally low dose levels to the fetus during early pregnancy.
3. The use of a lead apron or other added shielding does not lower substantially most of the dose to the organs and tissues of the body, but does reduce further the already minimal dose to the fetus.

Implications for Patient Care

1. Based on our Monte Carlo and phantom study, mammography can be considered as an option by radiologists faced with an early-stage pregnant patient with a possible diagnosis of breast cancer.
2. If mammography is performed on a pregnant patient, the use of a lead apron to further lower the dose to the fetus is advised.
3. If a patient is not aware of her pregnancy status and happens to undergo mammography, the risk to the fetus appears to be minimal.

Acknowledgements

The authors would like to thank Steve Pittard for providing technical assistance with the use of Emory University's High Performance Computer Cluster. This study was supported in part by the National Institutes of Health (NIH) grant RO1-EB004015 from the National Institute of Biomedical Imaging and Bioengineering (NIBIB). This work was also supported by a grant from the Georgia Cancer Coalition (GCC). The contents are solely the responsibility of the authors and do not necessarily represent the official views of the NIH, NIBIB or the GCC.

References

1. Hammerstein GR, Miller DW, White DR, Masterson ME, Woodard HQ, Laughlin JS. Absorbed radiation dose in mammography. Radiology 1979;130(2):485–491. [PubMed: 760167]
2. Dance DR. The Monte Carlo calculation of integral radiation dose in xeromammography. Phys Med Biol 1980;25(1):25–37. [PubMed: 7360790]
3. Doi K, Chan HP. Evaluation of absorbed dose in mammography: monte carlo simulation studies. Radiology 1980;135(1):199–208. [PubMed: 7360961]
4. Dance DR. Monte Carlo calculation of conversion factors for the estimation of mean glandular breast dose. Phys Med Biol 1990;35(9):1211–1219. [PubMed: 2236205]
5. Wu X, Barnes GT, Tucker DM. Spectral dependence of glandular tissue dose in screen-film mammography. Radiology 1991;179(1):143–148. [PubMed: 2006265]
6. Wu X, Gingold EL, Barnes GT, Tucker DM. Normalized average glandular dose in molybdenum target-rhodium filter and rhodium target-rhodium filter mammography. Radiology 1994;193(1):83–89. [PubMed: 8090926]
7. Boone JM. Glandular breast dose for monoenergetic and high-energy X-ray beams: Monte Carlo assessment. Radiology 1999;213(1):23–37. [PubMed: 10540637]
8. Boone JM. Normalized glandular dose (DgN) coefficients for arbitrary X-ray spectra in mammography: Computer-fit values of Monte Carlo derived data. Med Phys 2002;29(5):869–875. [PubMed: 12033583]
9. Behrman RH, Homer MJ, Yang WT, Whitman GJ. Mammography and Fetal Dose. Radiology 2007;243(2):605–606. [PubMed: 17456884]
10. Preston-Martin S, Pogoda JM. Estimation of radiographic doses in a case-control study of acute myelogenous leukemia. Health Phys 2003;84(2):245–259. [PubMed: 12553655]
11. Hatziioannou KA, Psarrakos K, Molyvda-Athanasopoulou E, et al. Dosimetric considerations in mammography. Eur Radiol 2000;10(7):1193–1196. [PubMed: 11003419]
12. Agostinelli S, Allison J, Amako K, et al. Geant4 - A simulation toolkit. Nucl Instrum Meth A 2003;506 (3):250–303.
13. Allison J, Amako K, Apostolakis J, et al. Geant4 Developments and Applications. IEEE Trans Nucl Sci 2006;53(1):270–278.
14. Description of the Mathematical Phantom. ORNL Center for Biokinetic and Dosimetric Research. [Accessed October 10, 2006]. http://ordose.ornl.gov/resources/phantom.html. Updated September 21, 2005
15. Cristy, M. Mathematical phantoms representing children of various ages for use in estimates of internal dose. Oak Ridge, Tennessee: Oak Ridge National Laboratory; 1980. ORNL/NUREG/ TM-367

16. Valentin J. Basic anatomical and physiological data for use in radiological protection: reference values - ICRP Publication 89. Ann ICRP 2002;32:1–277.
17. International Commission on Radiation Units and Measurements. ICRU report 46: Photon, electron, proton, and neutron interaction data for body tissues. Bethesda, Md., U.S.A.: International Comission on Radiation Units and Measurements; 1992.
18. Gray, H.; Goss, CM. Anatomy of the human body. Philadelphia, PA: Lea & Febiger; 1973.
19. Boone JM, Lindfors KK, Cooper VN 3rd, Seibert JA. Scatter/primary in mammography: Comprehensive results. Med Phys 2000;27(10):2408–2416. [PubMed: 11099211]
20. Sechopoulos I, Suryanarayanan S, Vedantham S, D'Orsi C, Karellas A. Computation of the glandular radiation dose in digital tomosynthesis of the breast. Med Phys 2007;34(1):221–232. [PubMed: 17278508]
21. Sechopoulos I, Suryanarayanan S, Vedantham S, D'Orsi CJ, Karellas A. Scatter radiation in digital tomosynthesis of the breast. Med Phys 2007;34(2):564–576. [PubMed: 17388174]
22. Young KC, Burch A. Radiation doses received in the UK Breast Screening Programme in 1997 and 1998. Br J Radiol 2000;73(867):278–287. [PubMed: 10817044]
23. Jamal N, Ng KH, McLean D. A study of mean glandular dose during diagnostic mammography in Malaysia and some of the factors affecting it. Br J Radiol 2003;76(904):238–245. [PubMed: 12711643]
24. International Commission on Radiation Units and Measurements. ICRU report 44: Tissue substitutes in radiation dosimetry and measurement. Bethesda, Md., U.S.A.: International Commission on Radiation Units and Measurements; 1989.
25. Wilkinson L, Heggie JCP. Glandular Breast Dose: Potential Errors. Radiology 2001;213:1.
26. Rosenstein, M. Handbook of selected organ doses for projections common in diagnostic radiology. Rockville, MD: Food and Drug Administration (FDA) Publication; 1976.
27. Kramer R, Drexler G. On the Calculation of the Effective Dose Equivalent. Radiat Prot Dosimetry 1982;3(1–2):13–24.
28. King SD, Spiers FW. Photoelectron enhancement of the absorbed dose from X rays to human bone marrow: experimental and theoretical studies. Br J Radiol 1985;58(688):345–356. [PubMed: 4063677]
29. Cristy, M.; Eckerman, K. Specific absorbed fractions of energy at various ages from internal photon sources. I. Methods. Oak Ridge, TN: Oak Ridge National Laboratory; 1987. Report ORNL/TM-8381/V1
30. Zankl M, Wittmann A. The adult male voxel model "Golem" segmented from whole-body CT patient data. Radiat Environ Biophys 2001;40(2):153–162. [PubMed: 11484787]
31. Kramer R, Vieira JW, Khoury HJ, Lima FRA, Fuelle D. All about MAX: a male adult voxel phantom for Monte Carlo calculations in radiation protection dosimetry. Phys Med Biol 2003;48(10):1239–1262. [PubMed: 12812444]
32. Kramer R, Khoury HJ, Vieira JW, et al. All about FAX: a Female Adult voXel phantom for Monte Carlo calculation in radiation protection dosimetry. Phys Med Biol 2004;49(23):5203–5216. [PubMed: 15656272]
33. Lee C, Lee C, Shah AP, Bolch WE. An assessment of bone marrow and bone endosteum dosimetry methods for photon sources. Phys Med Biol 2006;51(21):5391–5407. [PubMed: 17047259]
34. International Commission on Radiological Protection. ICRP Publication 60: 1990 recommendations of the International Commission on Radiological Protection. Oxford; New York: Published for the International Commission on Radiological Protection by Pergamon Press; 1991.
35. Draft Recommendations of the International Commission on Radiological Protection. International Commission on Radiological Protection. [Accessed February 2, 2007]. http://www.icrp.org/docs/ICRP_Draft_Recommendations_12_January_2007.pdf. Updated January 12, 2007
36. Grabski V, Brandan ME, Ruiz-Trejo C, Villasenor Y. SU-FF-I-34: PSF and S/P in Mammography: A Validation of Simulations Using the GEANT4 Code. Med Phys 2005;32(6):1911.
37. Sechopoulos I, Vedantham S, Suryanarayanan S, Karellas A. SU-FF-I-12: Validation of Geant4's Predictions On X-Ray Scatter and Glandular Dose in Pendant-Geometry Cone-Beam Breast CT. Med Phys 2006;33(6):1999–1999.

38. Boone JM, Fewell TR, Jennings RJ. Molybdenum, rhodium, and tungsten anode spectral models using interpolating polynomials with application to mammography. Med Phys 1997;24(12):1863–1874. [PubMed: 9434969]

39. International Commission on Radiological Protection. ICRP Publication 34: Protection of the patient in diagnostic radiology: a report of Committee 3 of the International Commission on Radiological Protection. Oxford; New York: Published for The Commission by Pergamon Press; 1982.

40. McWilliams A, Lam S. Lung cancer screening. Curr Opin Pulm Med 2005;11(4):272–277. [PubMed: 15928490]

41. Huda W, Scalzetti EM, Roskopf M. Effective doses to patients undergoing thoracic computed tomography examinations. Med Phys 2000;27(5):838–844. [PubMed: 10841385]

42. Winer-Muram HT, Boone JM, Brown HL, Jennings SG, Mabie WC, Lombardo GT. Pulmonary embolism in pregnant patients: fetal radiation dose with helical CT. Radiology 2002;224(2):487–492. [PubMed: 12147847]

43. Castellano IA, Dance DR, Evans PM. CT dosimetry: getting the best from the adult Cristy phantom. Radiat Prot Dosimetry 2005;114(1–3):321–325. [PubMed: 15933130]

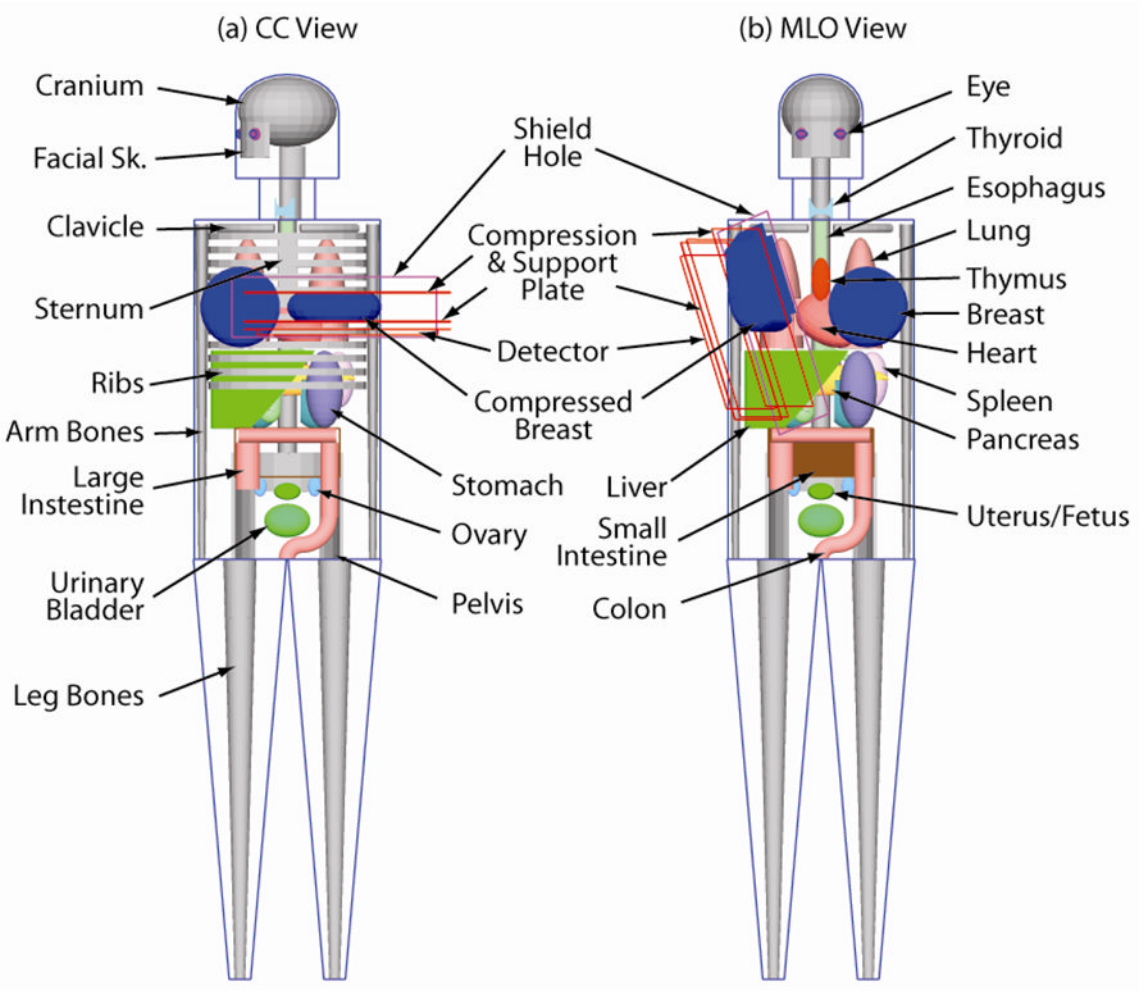

Fig 1.

Simulation geometry used in this study for the (a) CC view and (b) MLO view. In the CC view, only the small intestine's outline is included to show the pelvis. In the MLO view the rib cage and the sternum are omitted to show the other organs.

TABLE 1

List of organs, bones, skin sections and soft tissue volumes that compose the anthropomorphic phantom used in this study and their respective mass. The mass of each volume is per unit and is exclusive of contents.

	Name	Mass (g)
Organs	Adrenal	5.1
	Brain	1,407.6
	Breast	601.6
	Colon (ascending)	71.6
	Colon (transverse)	95.2
	Colon (descending)	70.4
	Colon (sigmoid)	55.4
	Esophagus	34.3
	Eye	6.6
	Eye Lens	0.2
	Gall Bladder	9.1
	Heart	242.7
	Kidney	125.2
	Liver	1,425.5
	Lung (left)	266.1
	Lung (right)	305.4
	Ovary	5.4
	Pancreas	64.9
	Pectoralis Muscle of Imaged Breast[1]	116.5
	Small Intestine	830.4
	Spleen	125.6
	Stomach	116.5
	Thymus	28.0
	Thyroid	12.1
	Urinary Bladder	35.5
	Uterus/Fetus	78.2
Skeleton	Arm Bone (lower section)[2]	173.6
	Arm Bone (middle section)[2]	145.1
	Arm Bone (upper section)[2]	193.0
	Clavicle	29.2
	Cranium	711.5
	Facial Skeleton	92.8
	Leg Bone (lower section)[2]	484.6
	Leg Bone (middle section)[2]	588.6
	Leg Bone (upper section)[2]	396.1
	Pelvis	644.0
	Rib Cage	725.8
	Scapulae	104.8
	Spine	1,059.1
	Sternum	58.1
Soft Tissue	Head	2,108.1
	Leg	7,033.0
	Neck	561.8
	Trunk	24,892.2
Skin	Breast	76.4
	Head	205.1
	Leg	514.5
	Neck	47.8
	Trunk	1,068.2

[1] NOTE: The pectoralis muscle simulated is only the portion inside the imaged compressed breast in the medio-lateral oblique view.

[2] Sections as defined in the description of the Cristy phantom (14)

TABLE 2

Dose to the organs, bones and skin sections per unit dose to the imaged breast (ROD) in the CC view. Only the volumes with a ROD higher than 0.10% in at least one view and one spectrum and the uterus/fetus are included. For the cases where the ROD was found to be equivalent for left and right imaged breast, the mean value is reported, for the other cases both ROD are shown (left/right). The first half value layer of the spectra is computed under the compression plate. Note that the ROD values for the uterus/fetus are not percentages.

	Volume	25 kVp 0.322 mm Al	Mo/Mo 30 kVp 0.378 mm Al	35 kVp 0.417 mm Al	25 kVp 0.371 mm Al	Mo/Rh 30 kVp 0.431 mm Al	35 kVp 0.465 mm Al	25 kVp 0.353 mm Al	Rh/Rh 30 kVp 0.442 mm Al	35 kVp 0.508 mm Al
Organs	Breast (CL)	0.40%	0.42%	0.45%	0.42%	0.44%	0.46%	0.43%	0.46%	0.49%
	Eye (IL)	0.02%	0.02%	0.02%	0.02%	0.02%	0.02%	0.02%	0.02%	0.03%
	Eye Lens (IL)	0.02%	0.02%	0.03%	0.02%	0.02%	0.03%	0.02%	0.02%	0.02%
	Heart	0.01%	0.03%/ 0.02%	0.08%/ 0.05%	0.02%	0.04%/ 0.03%	0.08%/ 0.05%	0.02%	0.06%/ 0.04%	0.09%/ 0.06%
	Lung (IL)	0.01%	0.03%/ 0.04%	0.07%/ 0.09%	0.02%	0.04%/ 0.05%	0.08%/ 0.09%	0.03%	0.06%/ 0.07%	0.09%/ 0.11%
	Thymus	0.02%	0.04%	0.08%	0.03%	0.05%	0.09%	0.04%	0.07%	0.10%
	Uterus or Fetus[1]	$<10^{-8}$	$<10^{-7}$	$<10^{-7}$	$<10^{-8}$	$<10^{-7}$	$<10^{-7}$	$<10^{-7}$	$<10^{-7}$	$<10^{-7}$
Bone Marrow	Clavicle (IL)	0.06%	0.07%	0.09%	0.07%	0.08%	0.10%	0.07%	0.09%	0.11%
	Rib Cage	0.08%	0.10%	0.13%	0.10%	0.12%	0.14%	0.11%	0.14%	0.17%
	Sternum	0.33%	0.38%	0.46%	0.38%	0.43%	0.49%	0.40%	0.49%	0.56%
Bone Surface	Arm Bone (middle section, IL)	0.07%	0.09%	0.12%	0.09%	0.10%	0.12%	0.09%	0.12%	0.15%
	Arm Bone (upper section, IL)	0.12%	0.14%	0.18%	0.14%	0.16%	0.19%	0.15%	0.19%	0.23%
	Clavicle (IL)	0.24%	0.29%	0.39%	0.29%	0.33%	0.40%	0.31%	0.39%	0.47%
	Rib Cage	0.32%	0.41%	0.55%	0.41%	0.49%	0.59%	0.45%	0.60%	0.72%
	Sternum	1.35%	1.59%	1.92%	1.58%	1.79%	2.04%	1.68%	2.05%	2.36%
Skin	Trunk	0.58%	0.54%	0.52%	0.53%	0.50%	0.49%	0.54%	0.49%	0.47%
	Neck	0.18%	0.15%	0.14%	0.15%	0.14%	0.13%	0.15%	0.13%	0.12%
	Head	0.63%	0.55%	0.51%	0.54%	0.49%	0.46%	0.55%	0.46%	0.42%
	Breast (CL)	1.98%	1.86%	1.79%	1.84%	1.75%	1.71%	1.84%	1.68%	1.62%
	Breast (IL)	245.36%	219.40%	204.01%	217.79%	198.17%	188.60%	218.05%	186.88%	172.32%

[1]Note: Fetus in the first trimester. ROD = Relative Organ Dose, CC = Cranio-Caudal, CL = Contralateral, IL = Ipsilateral

TABLE 3

Dose to the organs, bones and skin sections per unit dose to the imaged breast (ROD) in the MLO view. Only the volumes with a ROD higher than 0.10% in at least one view and one spectrum and the uterus/fetus are included. For the cases where the ROD was found to be equivalent for left and right imaged breast, the mean value is reported, for the other cases both ROD are shown (left/right). The first half value layer of the spectra is computed under the compression plate. Note that the ROD values for the uterus/fetus are not percentages.

	Volume	25 kVp 0.322 mm Al	Mo/Mo 30 kVp 0.378 mm Al	35 kVp 0.417 mm Al	25 kVp 0.371 mm Al	Mo/Rh 30 kVp 0.431 mm Al	35 kVp 0.465 mm Al	25 kVp 0.353 mm Al	Rh/Rh 30 kVp 0.442 mm Al	35 kVp 0.508 mm Al
Organs	Breast (CL)	0.51%	0.55%	0.57%	0.54%	0.56%	0.59%	0.55%	0.59%	0.62%
	Eye (IL)	0.07%	0.08%	0.08%	0.08%	0.08%	0.09%	0.08%	0.09%	0.10%
	Eye Lens (IL)	0.10%	0.11%	0.12%	0.12%	0.13%	0.14%	0.12%	0.14%	0.16%
	Heart	0.02%/ 0.01%	0.03%/ 0.01%	0.06%/ 0.03%	0.03%/ 0.01%	0.04%/ 0.02%	0.06%/ 0.03%	0.03%/ 0.01%	0.05%/ 0.02%	0.08%/ 0.03%
	Lung (IL)	0.02%	0.04%	0.08%/ 0.09%	0.03%/ 0.04%	0.05%/ 0.06%	0.08%/ 0.10%	0.04%/ 0.05%	0.07%/ 0.08%	0.10%/ 0.12%
	Pectoralis Muscle[1]	16.44%	18.55%	20.33%	18.94%	20.73%	21.91%	19.67%	22.95%	24.76%
	Thymus	0.01%	0.02%	0.06%	0.02%	0.03%	0.06%	0.03%	0.04%	0.07%
	Uterus or Fetus[2]	$<10^{-6}$	$<10^{-6}$	$<10^{-5}$	$<10^{-6}$	$<10^{-6}$	$<10^{-5}$	$<10^{-6}$	$<10^{-5}$	$<10^{-5}$
Bone Marrow	Clavicle (IL)	0.01%	0.02%	0.04%	0.02%	0.03%	0.04%	0.02%	0.04%	0.05%
	Rib Cage	0.11%	0.13%	0.16%	0.13%	0.15%	0.17%	0.14%	0.17%	0.20%
	Sternum	0.16%	0.18%	0.22%	0.18%	0.20%	0.23%	0.19%	0.23%	0.27%
Bone Surface	Arm Bone (middle section, IL)	0.00%	0.00%	0.01%	0.00%	0.00%	0.01%	0.00%	0.00%	0.01%
	Arm Bone (upper section, IL)	0.00%	0.01%	0.04%	0.01%	0.02%	0.04%	0.01%	0.02%	0.04%
	Clavicle (IL)	0.06%	0.10%	0.18%	0.09%	0.12%	0.18%	0.10%	0.15%	0.22%
	Rib Cage	0.44%	0.54%	0.68%	0.54%	0.62%	0.73%	0.58%	0.73%	0.84%
	Sternum	0.64%	0.75%	0.92%	0.74%	0.84%	0.97%	0.80%	0.96%	1.10%
Skin	Trunk	0.75%	0.69%	0.67%	0.69%	0.65%	0.63%	0.71%	0.64%	0.60%
	Neck	0.10%	0.09%	0.08%	0.09%	0.08%	0.08%	0.09%	0.08%	0.07%
	Head	0.14%	0.14%	0.13%	0.13%	0.13%	0.13%	0.14%	0.12%	0.12%
	Breast (CL)	2.25%	2.06%	1.95%	2.04%	1.90%	1.84%	2.05%	1.84%	1.74%
	Breast (IL)	170.13%	152.27%	141.52%	150.96%	137.44%	130.75%	150.79%	128.99%	118.73%

[1] Note: The pectoralis muscle simulated is the portion inside the imaged compressed breast.

[2] Fetus in the first trimester. ROD = Relative Organ Dose, MLO = Medio-Lateral Oblique, CL = Contralateral, IL = Ipsilateral

TABLE 4

Example computation of the total dose to the organs in microGy resulting from a standard two-view mammogram to one (left/right) breast, assuming 2 mGy glandular dose to the imaged breast for the CC view and 2.5 mGy glandular dose to the imaged breast for the MLO view, and using the data from Table 2 and 3. Divide the results in this table by 10 for conversion from microGy to mrad.

	Volume	25 kVp 0.322 mm Al	Mo/Mo 30 kVp 0.378 mm Al	35 kVp 0.417 mm Al	25 kVp 0.371 mm Al	Mo/Rh 30 kVp 0.431 mm Al	35 kVp 0.465 mm Al	25 kVp 0.353 mm Al	Rh/Rh 30 kVp 0.442 mm Al	35 kVp 0.508 mm Al
Organs	Breast (CL)	20.8	22.2	23.3	21.9	22.8	24.0	22.4	24.0	25.3
	Eye (IL)	2.2	2.4	2.4	2.4	2.4	2.7	2.4	2.7	3.1
	Eye Lens (IL)	2.9	3.2	3.6	3.4	3.7	4.1	3.4	3.9	4.4
	Heart	0.8/0.4	1.5/0.8	3.0/1.6	1.2/0.6	1.8/1.0	3.1/1.6	1.5/0.8	2.5/1.3	3.8/2.0
	Lung (IL)	0.7	1.5/1.8	3.5/4.1	1.2/1.4	2.0/2.3	3.6/4.1	1.5/1.9	2.8/3.3	4.4/5.2
	Pectoralis Muscle	411.0	463.8	508.2	473.6	518.2	547.8	491.8	573.8	619.0
	Thymus	0.7	1.3	3.1	1.1	1.8	3.3	1.6	2.4	3.8
	Uterus	<0.003	<0.003	<0.03	<0.003	<0.003	<0.03	<0.003	<0.03	<0.03
Bone Marrow	Clavicle (IL)	1.5	1.9	2.8	1.9	2.4	3.0	1.9	2.8	3.5
	Rib Cage	4.4	5.3	6.6	5.3	6.2	7.1	5.7	7.1	8.4
	Sternum	10.6	12.1	14.7	12.1	13.6	15.6	12.8	15.6	18.0
Bone Surface	Arm Bone (middle section, IL)	1.4	1.8	2.7	1.8	2.0	2.7	1.8	2.4	3.3
	Arm Bone (upper section, IL)	2.4	3.1	4.6	3.1	3.7	4.8	3.3	4.3	5.6
	Clavicle (IL)	6.3	8.3	12.3	8.1	9.6	12.5	8.7	11.6	14.9
	Rib Cage	17.4	21.7	28.0	21.7	25.3	30.1	23.5	30.3	35.4
	Sternum	43.0	50.6	61.4	50.1	56.8	65.1	53.6	65.0	74.7
Skin	Trunk	30.3	28.1	27.0	27.9	26.3	25.7	28.6	25.8	24.4
	Neck	6.2	5.2	5.0	5.3	4.7	4.5	5.3	4.6	4.2
	Head	16.2	14.4	13.4	14.2	13.0	12.4	14.5	12.2	11.4
	Breast (CL)	95.8	88.6	84.6	87.9	82.4	80.1	88.1	79.6	75.9
	Breast (IL)	9160.4	8194.7	7618.2	8130.0	7399.5	7040.6	8130.8	6962.4	6414.7

[1] Note: Fetus in the first trimester. MLO = Medio-Lateral Oblique, CC = Cranio-Caudal, CL = Contralateral, IL = Ipsilateral

TABLE 5

Coefficients of variation of ROD for the left breast after 5 independent Monte Carlo simulations.

	X-ray Spectrum View	Mo/Mo 25 kVp		Rh/Rh 35 kVp	
		CC	MLO	CC	MLO
Organs	Breast (CL)	0.17%	0.14%	0.12%	0.06%
	Eye (IL)	6.89%	3.07%	4.26%	2.92%
	Eye Lens (IL)	31.55%	13.68%	27.02%	5.67%
	Heart	1.62%	0.93%	0.30%	0.26%
	Lung (IL)	1.01%	0.71%	0.28%	0.28%
	Pectoralis Muscle	-	0.07%	-	0.03%
	Thymus	4.02%	3.24%	1.05%	1.01%
	Uterus	124.43%	45.46%	8.55%	4.71%
Bone Marrow	Clavicle (IL)	0.34%	1.62%	0.48%	0.51%
	Rib Cage	0.09%	0.15%	0.05%	0.06%
	Sternum	0.15%	0.33%	0.30%	0.07%
Bone Surface	Arm Bone (middle section, IL)	0.21%	7.75%	0.41%	0.30%
	Arm Bone (upper section, IL)	0.54%	1.36%	0.34%	0.64%
	Clavicle (IL)	0.37%	1.63%	0.47%	0.52%
	Rib Cage	0.09%	0.15%	0.06%	0.06%
	Sternum	0.15%	0.33%	0.29%	0.07%
Skin	Trunk	0.42%	0.40%	0.61%	0.31%
	Neck	0.39%	0.58%	0.39%	1.24%
	Head	0.38%	0.54%	0.39%	0.48%
	Breast (CL)	0.20%	0.34%	0.44%	0.53%
	Breast (IL)	0.35%	0.19%	0.28%	0.35%

ROD = Relative Organ Dose, CC = Cranio-Caudal, MLO = Medio-Lateral Oblique, CL = Contralateral, IL = Ipsilateral

TABLE 6

Efficiency of the virtual lead shield measured by $ROD_{Shield}/ROD_{No\ Shield}$ The values presented are the mean values for all spectra and both breasts.

		View	
		CC	**MLO**
Organs	Breast (CL)	0.943	0.285
	Eye (IL)	0.024	0.040
	Eye Lens (IL)	0.082	0.031
	Heart	0.998	0.841
	Lung (IL)	0.968	0.984
	Pectoralis Muscle	N/A	1.000
	Thymus	0.914	0.676
	Uterus	0.139	0.483
Bone Marrow	Clavicle (IL)	0.004	0.446
	Rib Cage	0.761	0.839
	Sternum	0.711	0.257
Bone Surface	Arm Bone (middle section, IL)	0.995	0.882
	Arm Bone (upper section, IL)	0.730	0.983
	Clavicle (IL)	0.004	0.448
	Rib Cage	0.761	0.839
	Sternum	0.711	0.258
Skin	Trunk	0.483	0.725
	Neck	0.002	0.054
	Head	0.003	0.067
	Breast (CL)	0.936	0.259
	Breast (IL)	1.000	1.000

ROD = Relative Organ Dose, CC = Cranio-Caudal, MLO = Medio-Lateral Oblique, CL = Contralateral, IL = Ipsilateral